

Optical-Clock-Based Time Scale

Jian Yao,^{*} Jeff A. Sherman, Tara Fortier, Holly Leopardi, Thomas Parker, William McGrew, Xiaogang Zhang, Daniele Nicolodi, Robert Fasano, Stefan Schäffer, Kyle Beloy, Joshua Savory, Stefania Romisch, Chris Oates, Scott Diddams, Andrew Ludlow, and Judah Levine

Time and Frequency Division, National Institute of Standards and Technology, Boulder, Colorado, 80305, USA



(Received 10 April 2019; revised manuscript received 28 August 2019; published 30 October 2019)

A time scale is a procedure for accurately and continuously marking the passage of time. It is exemplified by Coordinated Universal Time (UTC) and provides the backbone for critical navigation tools such as the Global Positioning System. Present time scales employ microwave atomic clocks, whose attributes can be combined and averaged in a manner such that the composite is more stable, accurate, and reliable than the output of any individual clock. Over the past decade, clocks operating at optical frequencies have been introduced that are orders of magnitude more stable than any microwave clock. However, in spite of their great potential, these optical clocks cannot be operated continuously, which makes their use in a time scale problematic. We report the development of a hybrid microwave-optical time scale, which only requires the optical clock to run intermittently while relying upon the ensemble of microwave clocks to serve as the flywheel oscillator. The benefit of using a clock ensemble as the flywheel oscillator instead of a single clock can be understood by the Dick-effect limit. This time scale demonstrates for the first time subnanosecond accuracy over a few months, attaining a fractional frequency stability of 1.45×10^{-16} at 30 days and reaching the 10^{-17} decade at 50 days, with respect to UTC. This time scale significantly improves the accuracy in timekeeping and could change the existing time-scale architectures.

DOI: 10.1103/PhysRevApplied.12.044069

I. INTRODUCTION

Time is a dimension in which events can be ordered from the past through the present and into the future. Many modern-day technologies rely on the ability to do this accurately and precisely, including navigation [1], telecommunication systems [2], electrical power grids [3], and even electronic transactions on the stock exchange [4]. The most advanced timekeeping can be applied to fundamental science studies [5], such as searches for dark matter [6] and neutrino speed measurements [7].

The microwave frequency of exactly 9.192 631 770 GHz, corresponding to the transition between the two hyperfine levels of the ground state of the cesium atom, has defined the International system of units (SI) second since 1967 [8], and such microwave clocks are the basis of international time. In practical timekeeping systems, an ensemble of atomic clocks based on cesium, hydrogen, and rubidium is usually used. Commercially available cesium, hydrogen, and rubidium clocks typically exhibit the fractional frequency stabilities [9] of 8.5×10^{-12} [10], 1.0×10^{-13} [11], and 1.5×10^{-12} [12] over 1 second of averaging, respectively. The clock ensemble forms a time scale with better performance and reliability than that afforded by an individual clock [13]. Within

this context, a new generation of atomic clocks, based instead on optical frequencies, have shown potential for tremendous improvement in timekeeping [14]. Examples of optical clock species include Yb⁺ [15], Al⁺ [16], Yb [17,18], and Sr [19], with corresponding fractional frequency stabilities of 5.0×10^{-15} , 2.0×10^{-15} , 1.4×10^{-16} , and 3.1×10^{-16} at 1 second have been demonstrated, representing orders-of-magnitude improvement over the best microwave clocks. Note, in the following context, we may use “frequency” to stand for “fractional frequency” for simplicity, which can be easily identified from the dimensionless unit.

However, a key challenge is that these experimental optical clocks do not yet operate continuously for long intervals such as several days, making it difficult to incorporate them into conventional time scales. Recent efforts explore the combination of an intermittent optical clock with a continuous hydrogen maser for time-scale generation [20–23]. As outlined in the green dashed box of Fig. 1(a), the optical clock provides occasional frequency corrections to the hydrogen maser to counteract its tendency to drift. In this “hydrogen maser + optical clock” (HMOC) architecture, the performance is limited by the noise of the hydrogen maser and the operation time of the optical clock. This intrinsic limitation has been explored theoretically for different conditions with numerical simulation [24], and can be further understood as an aliasing

*jian.yao@colorado.edu

phenomenon of maser noise periodically sampled by the optical clock, referred to as the Dick effect (Appendix A).

This paper explores an alternative way to improve an optical-clock-based time scale independent of the optical-clock operation time: improving the stability of the flywheel oscillator. We propose steering an ensemble of microwave clocks (e.g., a few hydrogen masers), instead of a single hydrogen maser, to an optical clock, [see the red dashed box of Fig. 1(a)]. Because the microwave time scale exhibits smaller noise than a single clock due to averaging, Dick-effect limitations in the steering process are reduced (Appendix A). This has also been confirmed by numerical simulation [24]. There, we show that the stability of the optical-clock-based time scale is proportional to the square root of the number of hydrogen masers. This “microwave time scale + optical clock” (MTSOC) architecture affords a time scale with improved performance at all averaging times, offering a complementary enhancement to that realized with increased optical-clock uptime. As an example, to achieve the performance of 4.0×10^{-17} at 10^7 s (i.e., time deviation of 0.23 ns at 10^7 s), we can reduce the uptime of an optical clock from 50% to 8% by increasing the maser number from one to six [Fig. 1(b)].

To test the MTSOC architecture, we conduct a campaign at NIST (National Institute of Standards and Technology, USA) from October 2017 to April 2018. Over the five months, the Yb clock operated intermittently for an average of 1.5 h per day. The free-running microwave time scale AT1, composed of a few hydrogen masers and a few commercial cesium clocks, is steered to the Yb clock using a Kalman filter. We show that the MTSOC architecture exhibits unprecedented timing accuracy (0.40 ns, root-mean-square variation) and frequency stability (1.45×10^{-16} at 30 days, 8.8×10^{-17} at 50 days), despite only 6% optical-clock availability. These results highlight a robust and realistic approach to immediately capitalize on the enhanced stability of the best optical clocks for international timekeeping. Moreover, our architecture is flexible and could further benefit from the addition of other optical clocks and stable laser oscillators [25,26] for better performance.

II. EXPERIMENTAL SCHEME OF OPTICAL-CLOCK-BASED TIME SCALE

Figure 2 shows the experimental details of the optical-clock-based time scale (i.e., AT1' time scale) based on

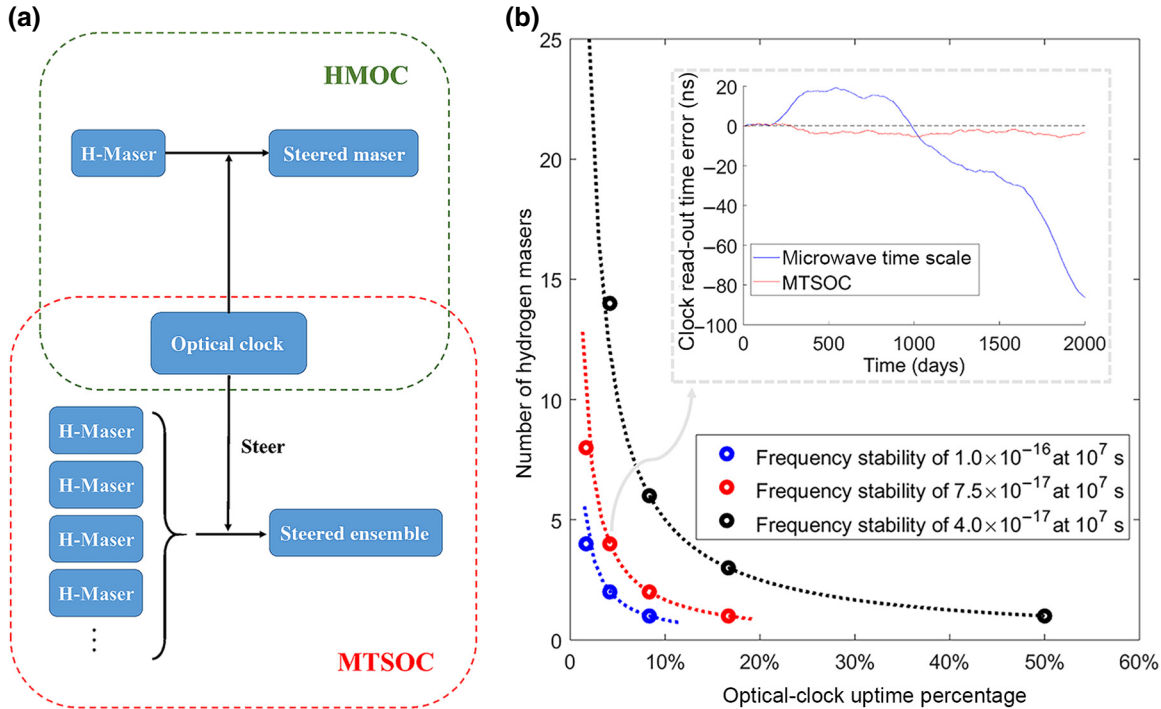


FIG. 1. Concept of an optical-clock-based time scale. (a) Illustrates the HMOC architecture (green dashed box) and the MTSOC architecture (red dashed box). (b) Summarizes the relation between the number of masers and the optical-clock uptime for different performance goals (blue, 1.0×10^{-16} at 10^7 s; red, 7.5×10^{-17} at 10^7 s; black, 4.0×10^{-17} at 10^7 s), when an optical clock runs once a day. The dots are the results of simulations, and the dashed curves are hyperbolas, which well fit the dots. The inserted plot of (b) shows an example of the simulation in time series. The blue solid curve is the read-out time error of a microwave time scale composed of four hydrogen masers, and the red solid curve is the read-out time error of a MTSOC composed of the four hydrogen masers and an optical clock of 4.2% uptime. Note (b) is plotted based on the simulations in [24].

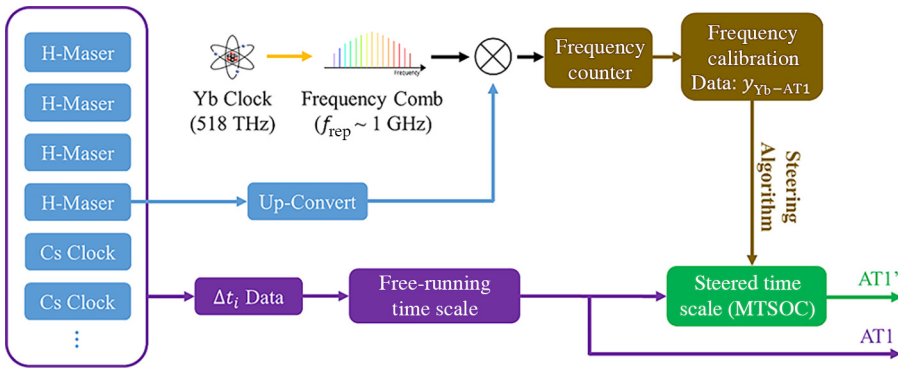


FIG. 2. Experimental scheme of optical-clock-based time scale AT1' and comparison to free-running time scale AT1.

the MTSOC architecture. An Yb optical-lattice clock, based on a $^1S_0 \rightarrow ^3P_0$ optical transition frequency of $518\,295\,836\,590\,863.71\text{ Hz} \pm 0.11\text{ Hz}$ [27], is used to stabilize a Ti:sapphire optical frequency comb [28]. The realization of the stabilization can be illustrated by Eq. (1).

$$f_{\text{laser}} = f_0 + n \cdot f_{\text{rep}} + f_{\text{beat}}, \quad (1)$$

where f_{laser} is the frequency of the laser signal that is frequency doubled and locked to the Yb atom's quantum transition. The comb's carrier-envelope offset frequency f_0 is locked to 10 MHz. n is an integer. f_{rep} is the frequency comb's repetition frequency, which is in the microwave region (close to 1 GHz). The beat frequency between the Yb-stabilized laser and the nearest comb tooth f_{beat} is locked to 640 MHz.

By Eq. (1), the Ti:sapphire frequency comb converts the Yb clock signal to the microwave region via generating the repetition frequency f_{rep} . This microwave signal is compared with an up-converted hydrogen maser signal at 1 GHz via a mixer. The maser used in this experiment is labeled ST15 at NIST and provides the reference for all locked comb beat notes. The frequency difference between the two microwave signals is measured by two frequency counters: a software-defined-radio counter [29] and a commercial frequency counter. The Yb clock is run in normal operation with a formal accounting of systematic clock shifts, including the gravitational redshift correction due to the height of the Yb clock from the geoid, with a total uncertainty below 1×10^{-17} . Offsets in the frequency-comb-based optical-to-microwave synthesis are characterized and confirmed to be small ($< 3 \times 10^{-17}$), and the frequency counters exhibit negligible bias ($< 1 \times 10^{-17}$).

From the frequency counter data, we derive the fractional frequency difference between the Yb clock and the hydrogen maser, that is, $y_{\text{Yb-HMaser}}$. As proposed in Sec. I, the MTSOC architecture is more favorable than the HMOC architecture, because the free-running microwave time scale is less noisy than the maser, which allows more aggressive steering. We observe that the existing microwave time scale AT1 (with at least six member masers) is more stable than a single hydrogen maser by

a factor of approximately 2. Another advantage of this architecture is that it is more reliable than the HMOC architecture because the time scale is only minimally affected by the failure of one of its contributing member clocks [13]. To achieve the MTSOC architecture, we need to know the fractional frequency difference between Yb and AT1, $y_{\text{Yb-AT1}}$. Because ST15 is a member clock in AT1, and we continuously monitor the fractional frequency difference between this maser and AT1 (i.e., $y_{\text{HMaser-AT1}}$), we can compute $y_{\text{Yb-AT1}}$ using the following equation.

$$y_{\text{Yb-AT1}} = y_{\text{Yb-HMaser}} + y_{\text{HMaser-AT1}}. \quad (2)$$

With the information of $y_{\text{Yb-AT1}}$, we can correct the frequency and frequency-drift error in AT1 using a Kalman filter and thus generate the MTSOC time scale; we name this output AT1'. The details of the Kalman-filter steering are discussed in Appendix B. We want to emphasize that AT1', designed for real-time implementation, is available for immediate use.

III. RESULTS OF THE CAMPAIGN IN MJD 58054–58214

The Yb clock ran regularly during the period of late October 2017 – early April 2018 (modified Julian date 58054–58214). Individual run times range from tens of seconds to several hours, depending on the experimental arrangement; no valid data are discarded. The total running time of the Yb clock is 241.8 h. We obtain the average frequency difference $y_{\text{Yb-AT1}}$ for each run using Eq. (2), the results of which are plotted in Fig. 3(a). $y_{\text{Yb-AT1}}$ is around -4.26×10^{-13} , with a scatter of approximately $\pm 5 \times 10^{-15}$. Note that this nonzero frequency difference comes from the frequency offset of AT1; because AT1 is a free-running time scale, no attempt is made to keep its frequency accurate.

The frequency stability $\sigma_{\text{Yb-AT1}}$ at an averaging time τ gives the statistical uncertainty of the average frequency difference $y_{\text{Yb-AT1}}$ as a function of τ . Therefore, the error bars in Fig. 3(a) are assigned based on $\sigma_{\text{Yb-AT1}}$ at τ equal to each run's duration. In general, shorter Yb clock runs result in a larger error bar. The computation of $\sigma_{\text{Yb-AT1}}$ is not

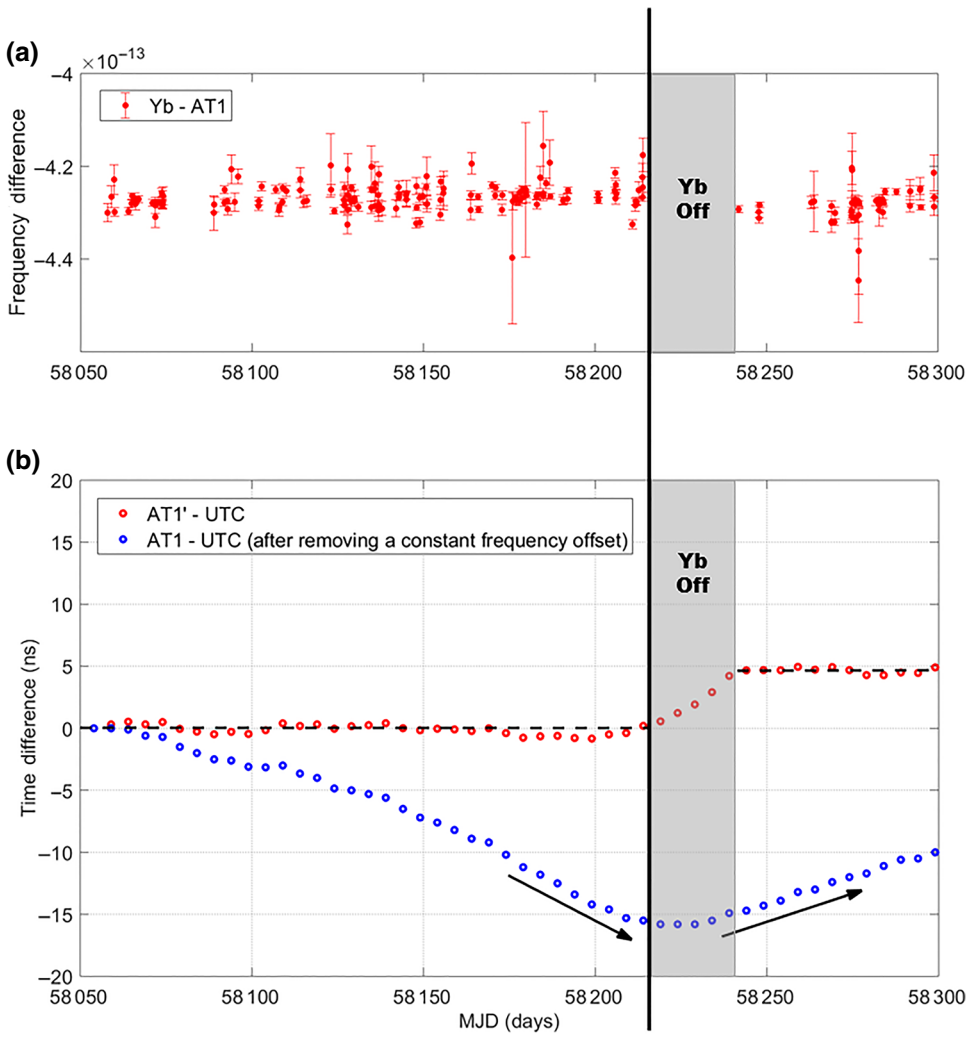


FIG. 3. (a) Shows the fractional frequency difference between the Yb clock and AT1 during MJD 58054–58214. Note AT1, composed of a few hydrogen masers and a few commercial cesium clocks, is a free-running microwave time scale at NIST. (b) Shows the time difference between AT1' and UTC (red dots) during MJD 58054–58214. AT1' is the NIST time scale that is steered to the Yb clock. AT1' is set to 0 ns initially. AT1' has a root-mean-square variation of 0.4 ns with respect to UTC during MJD 58054–58214. The time difference between AT1 and UTC (blue dots) is shown for reference. A constant frequency offset of $+4.278 \times 10^{-13}$ (measured from the first two points on the plot) in AT1 has already been removed. (c),(d) Show the behavior of AT1' and AT1 during MJD 58215–58300. During MJD 58215–58240 (gray region), the Yb clock ceases regular operation. After Yb-clock data resumes on MJD 58241, AT1' becomes flat with respect to UTC [black dashed line in (d)] indicating prompt frequency recalibration. The frequency change of AT1 is illustrated by the black arrows.

trivial and is determined in segments τ less than 12 min, τ between 12 min to 2 h, and $\tau > 2$ h. Considering that AT1 is computed on a 12-min grid [13], if the Yb clock runs for less than 12 min, σ_{Yb-AT1} is essentially $\sigma_{Yb-HMaser}$, which can be calculated using the $y_{Yb-HMaser}$ data. Since $\sigma_{Yb-HMaser}$ increases significantly as the averaging time decreases because of the white-phase noise process, it is necessary to run the Yb clock for at least tens of seconds. σ_{Yb-AT1} for intervals between 12 min and 2 h can be calculated straightforwardly: with a long (e.g., at least 6 h) dataset of y_{Yb-AT1} , we are able to calculate the frequency stability of σ_{Yb-AT1} up to 1/3 of the operation time with statistical confidence; multiple long datasets are used for the same calculation to improve the confidence. For the case of runs longer than 2 h, this calculation does not work as we do not have datasets lasting many hours. Nevertheless, we know that σ_{Yb-AT1} is composed of independent noise components σ_{Yb} , which is negligible, $\sigma_{\text{measurement}}$, which becomes negligible as well after 2 h based on the experimental data, and σ_{AT1} . Thus, we use σ_{AT1} to determine the error bar for Yb clock runs > 2 h. For intervals between

2 h and several days, σ_{AT1} is computed by a three-corner-hat analysis with two independent hydrogen masers not in AT1 (see Supplement of Ref. [27]).

Based on the y_{Yb-AT1} result in Fig. 3(a), we steer frequency and frequency drift parameters of AT1 to Yb immediately after each Yb run using the Kalman filter in Appendix B, generating the steered time scale AT1'. A new Yb clock run typically earns a weight of 5%–20%, depending on the duration of the new run and the elapsed interval since the last run. We derive the time difference between AT1' and AT1 by integrating the frequency and frequency drift steering record.

To evaluate the performance of AT1', we compare AT1' to Coordinated Universal Time (UTC) computed by the International Bureau of Weights and Measures (BIPM) via the chain of AT1' → AT1 → UTC(NIST) → UTC. Because $y_{AT1'-UTC}$ includes noise due to AT1', UTC, and the frequency chain, the frequency stability $\sigma_{AT1'-UTC}$ gives an upper limit on the stability of AT1'. In fact, the frequency stability of UTC is superb, since UTC receives contributions from multiple state-of-the-art Cs fountains

that define the SI second. Also, the links AT1'→AT1 and AT1→UTC(NIST) add negligible noise. Although the link UTC(NIST)→UTC suffers significant noise of approximately 4×10^{-16} over 5 days of averaging due to long baseline time-transfer methods [30,31], this link noise becomes negligible after approximately 10 days of averaging since the time-transfer noise is dominated by a flicker-phase process while the UTC–AT1' noise is mainly a white-frequency or flicker-frequency process. Taking these points into account, $\sigma_{\text{AT1}'-\text{UTC}}$ should be dominated by the noise in AT1' after averaging intervals of 10 days. In other words, the comparison between AT1' and UTC via the above chain is a valid method of evaluating the long-term (≥ 10 days) performance of AT1'.

In Fig. 3(b), red dots show the time difference between the optical-clock-based AT1' and UTC during the campaign (i.e., MJD 58054–58214). For comparison, blue dots show the time difference between AT1 and UTC with a constant frequency offset of $+4.278 \times 10^{-13}$ removed. We observe that AT1 walks away from UTC by approximately 16 ns over 160 days due to frequency drift in the free-running AT1. In contrast, AT1' is only 0.2 ns away from UTC after 160 days, indicating an average fractional frequency offset of 1.4×10^{-17} and an average fractional frequency drift of below $2.1 \times 10^{-24} \text{ s}^{-1}$. The maximum time error or the peak-to-peak time variation is another important aspect for a time scale. AT1' shows a peak-to-peak variation of 1.4 ns. AT1' exhibits a maximum time error of 0.8 ns and a time variation of 0.4 ns in root-mean-square, demonstrating subnanosecond accuracy.

Besides the above time-series comparison between AT1' and AT1, we also compare frequency stabilities for this campaign (Fig. 4). The stability of AT1' is comparable to that of AT1 for an averaging time of less than 20 days. After 20 days, AT1' significantly outperforms AT1. AT1' reaches 1.45×10^{-16} at 30 days and 8.8×10^{-17} at 50 days; in contrast, AT1 is 2.5×10^{-16} at 30 days and 3.5×10^{-16} at 50 days. The frequency stability of UTC(NIST) is shown for comparison. Because UTC(NIST) is usually steered to UTC weekly or biweekly for time accuracy, it exhibits worse short-term stability than AT1. However, this steering does accomplish better stability than AT1 over longer intervals. It is noteworthy that over all intervals AT1'—with just the benefit of Yb optical-clock frequency calibrations—exhibits an improvement of a factor of 2 in the frequency stability over UTC(NIST), which has the benefit of UTC informed time corrections.

The performance of existing Cs or Rb fountain-based time scales, which are among the world's best, is also provided for comparison. At PTB (Physikalisch-Technische Bundesanstalt, Germany), during the same time period (i.e., MJD 58054–58214), two Cs fountain clocks [32] operated nearly 100% of the time. The time scale UTC(PTB) is composed of these two Cs fountain clocks

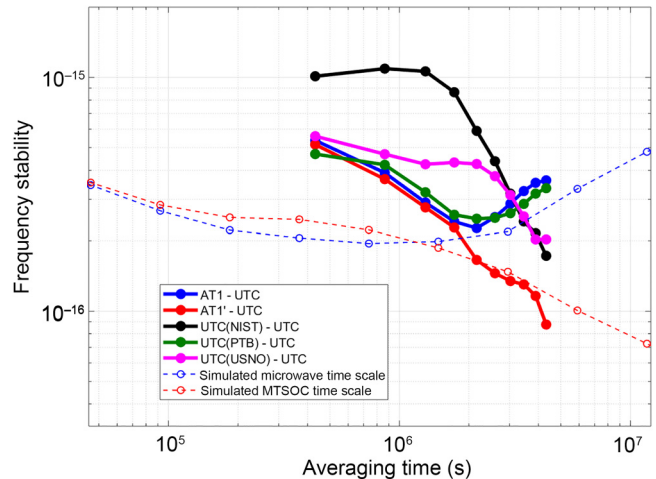


FIG. 4. Frequency stability of AT1, AT1', UTC(NIST), UTC(PTB), and UTC(USNO), for MJD 58054–58214. The frequency stability is characterized by modified total deviation, and error bars (omitted here for plot clarity) are provided in Appendix C. The dashed curves show the simulation result. Note, the simulated MTSOC time scale (red dashed curve) is composed of the simulated microwave time scale (blue dashed curve) and a simulated optical clock that runs one hour per day.

and a few hydrogen masers and is gently steered to UTC in the long term for time accuracy. UTC(PTB) exhibits a peak-to-peak variation of 3.5 ns over the whole 160 days with respect to UTC, which is larger than that of AT1'. The frequency stability of UTC(PTB) is 2.5×10^{-16} at 30 days and 3.4×10^{-16} at 50 days (green curve in Fig. 4). Similarly, at USNO (United States Naval Observatory), four Rb fountain clocks (with performance comparable to Cs fountains [33]) are running nearly 100% of the time. UTC(USNO), composed of the four Rb fountain clocks and dozens of hydrogen masers, has a peak-to-peak variation of 3.5 ns with respect to UTC and a frequency stability of 3.8×10^{-16} at 30 days and 2.0×10^{-16} at 50 days (magenta curve in Fig. 4).

IV. DISCUSSIONS

A. AT1' behavior in the absence of an optical clock

Presently, there is no guarantee that an optical clock at NIST will operate once every few days. Here, we explore AT1' behavior when the optical clock stops running for an extended period and is subsequently reintroduced; such a gap was present from April 7, 2018 (MJD 58215) – May 2, 2018 (MJD 58240) [see Figs. 3(c) and 3(d)]. Intuitively, when an optical clock stops running, AT1' should degrade to AT1. However, since AT1' keeps its latest frequency and frequency-drift steering parameters, its exact time evolution can differ from AT1. Coincidentally, AT1 experienced a random (statistical) positive frequency fluctuation during the data gap due to its intrinsic divergent behavior (annotated with black arrows in Fig. 3). AT1', lacking Yb

optical-clock calibrations, accumulated a positive time offset of approximately 5 ns accordingly. Upon resumption of the Yb optical clock on MJD 58241, we see that AT1' quickly corrected its frequency and time error ceased accumulating. We emphasize that the reason why AT1' time error does not become zero after MJD 58241 is that the Yb clock serves as a frequency standard instead of a time standard. In the latter period of regular Yb optical-clock runs (MJD 58241–58300), AT1' exhibits a peak-to-peak time variation of 0.7 ns and a root-mean-square time variation of 0.2 ns, consistent with the subnanosecond observation of AT1' discussed in Sec. III.

Based on these observations, to maintain time and frequency accuracy in AT1', it is necessary that the optical clock reference run at least occasionally, such as 6 h per week. We speculate that the required run schedule may be somewhat relaxed via use of a free-running timescale with better long-term stability (e.g., [34]).

B. Comparison between the real-data result and simulation

Over the period of MJD 58054–58214, the Yb clock is operated and measured an average of 1.5 h per day. Considering the nonuniform run schedule over that time (e.g., no weekend Yb clock operation), which degrades the performance of the optical-clock-based time scale, the real situation is more comparable to a simulation of running an optical clock one hour every day. The dashed curves in Fig. 4 are the simulation result for which we assume a noiseless reference time and no time-transfer noise. To be specific, the blue dashed curve is the simulated microwave time scale that represents AT1, while the red dashed curve is the simulated MTSOC result with an optical clock operating one hour per day.

By comparing the simulation result with the real-data result in Fig. 4, we see that the real-data result is noisier through approximately 10 days of averaging. We attribute this to the lack of time transfer and reference (i.e., UTC) noise in the simulations. The MTSOC architecture exhibits a significant improvement over the microwave time scale after 25 days in both simulation and real data. The divergence of the red curve from the blue curve in both simulation and real data indicates that the benefit of having an online calibration by an optical clock grows with time. Furthermore, both simulation and real data indicate that the MTSOC stability reaches the 10^{-17} regime after approximately 50 days. These observations generally validate the simulation results.

C. Future time keeping

From both simulation and observed data, it is clear that a better flywheel oscillator (i.e., maser ensemble) offers an optical-clock-based time scale improved stability. Following this same logic, other types of flywheel

oscillators under development may offer better performance still. For example, incorporating next-generation low-drift cavity stabilized lasers [25,26] into the flywheel ensemble could eventually yield a frequency stability of approximately 1×10^{-17} .

Alternatively, as noted earlier, higher optical-clock availability also offers time scale improvements. For example, with a consistent optical-clock availability at the 50% level, simulations indicate that our optical-clock-based time scale [24] could reach or exceed low 10^{-17} stability at approximately 100 days. While work is underway to develop an optical clock with high uptime, another path of increasing the optical-clock availability is to arrange for multiple optical clocks to contribute to AT1'. Indeed, as researchers explore the best optical clock candidates, many laboratories have developed more than one type of optical clock. Here at NIST, the Yb optical-lattice clock (featured above), the Al⁺ trapped-ion quantum-logic clock, and the JILA Sr optical-lattice clock could help calibrate AT1'. Even with only intermittent operation of each clock, a better long-term stability of AT1' results as the total optical-clock availability increases. This type of composite optical reference has the added advantage of redundancy: it is unlikely that multiple optical clocks would have long coincident periods of unavailability, avoiding the accumulation of large time error.

Beyond better local timekeeping, optical clocks offer improvements to International Atomic Time (TAI) and UTC [35]. Together with emerging time transfer techniques [29,35–39], global time accuracy could reach the subnanosecond level. This level of performance has the potential to benefit a range of other technologies, including gravimetry, global navigation satellite system (GNSS) positioning, deep space navigation, and telecommunication. As pointed out in [41,42], the most accurate time constitutes a key element in the development of alternative gravitational measurement techniques. Remote comparisons of time could help a relativistic determination of gravitational potential. Subnanosecond time accuracy at the ground monitoring stations could enable the estimation of the GNSS satellite clocks' time offsets with a smaller uncertainty, reducing an error source due to satellite clocks in precise positioning [43]. In deep space cruise navigation, range and Doppler data are collected from a single deep space network antenna over an observation interval typically lasting 8 h or more, with the next interval available several days to a week later [44]. A batch of observations over weeks to months are then used to solve for the trajectory. In this scenario, a subnanosecond ground time scale could help reduce the trajectory uncertainty coming from the reference-time uncertainty (without requiring the development of a stable space clock as suggested in [44]). Finally, it is interesting to note that in telecommunication, the performance requirement of primary reference clocks has evolved from the frequency uncertainty of 1×10^{-11} in

1988 (International Telecommunication Union Telecommunication Standardization Sector (ITU-T) G.811), to the time uncertainty of 100 ns in 2012 (ITU-T G.8272), and then further tightened to 30 ns in 2016 (ITU-T G.8272.1) [45]. Following this trend, one can expect this requirement to drop to a few ns in coming years, which can be challenging for the existing microwave time scales to support. In contrast, the performance of MTSOC as shown in this paper can fulfill this future requirement.

V. CONCLUSION

This paper presents an optical-clock-based time scale composed of an ensemble of continuously operating microwave clocks and an intermittently operating Yb optical clock. This time scale, AT1', shows a root-mean-square variation of 0.40 ns with respect to UTC for more than 5 months; its frequency stability is 1.45×10^{-16} at 30 days and reaches the 10^{-17} regime at 50 days. This level of performance would allow national metrology institutes to provide more accurate time. With more optical clocks contributing to AT1', the availability of optical data can be increased, yielding even better long-term stability. To further improve the performance of AT1', we anticipate incorporating high-performance optical cavities into the clock ensemble.

ACKNOWLEDGMENTS

We thank David Howe for the discussion on the frequency stability analysis. We also thank Neil Ashby and Victor Zhang for their helpful inputs.

Contribution of NIST – not subject to U.S. copyright.

Appendix A: Dick-effect limits on an optical-clock-based time scale

The general problem of locking a noisy oscillator to a reference in the presence of dead time (intervals where

no comparison data is present) has been considered extensively in the atomic clock community, and the frequency stability limits due to dead time are generally referred to as the Dick limit [46]. Armed with the noise spectrum of a local oscillator and the details of the dead time distribution and measurement periodicity, it is straightforward to calculate the Dick limit, which is typically relevant for long averaging intervals. Indeed, Dick-effect considerations have been a key motivating force behind the development of improved optical local oscillators from cavity stabilization [17].

Here, we consider the Dick-limited frequency stability in the context of locking the frequency of a maser ensemble to that of an optical clock when the optical clock is operated intermittently. We start with the simulated maser noise in [24]. To simplify the clock model, we assume that the maser is composed of a white frequency noise of 1.26×10^{-13} at 1 s, a flicker frequency noise of 3.09×10^{-16} at 1 s, and a random walk frequency noise of 2.44×10^{-19} at 1 s. This model represents the hydrogen maser behavior well for averaging intervals larger than 10 000 s. Based on these parameters, we calculate the maser's frequency noise power spectrum. This noise spectrum is the primary input in the Dick-effect calculation, which computes the aliasing of the maser noise into the optical clock based on how frequently the measurements are made and with what dead time exists between measurements.

For the case of an optical clock run once per day, the analytically derived Dick limits are plotted by the dashed lines in Fig. 5 for different scenarios. Note that the Dick effect results in a white frequency noise process, which is plotted here for all times, but is really just relevant at longer times (e.g., 10^7 s) where it would likely dominate the resulting frequency stability. We compare these Dick limits to the simulation results (solid curves) by focusing our attention at sufficiently long averaging intervals, for example 10^7 s, where the Dick effect would likely dominate

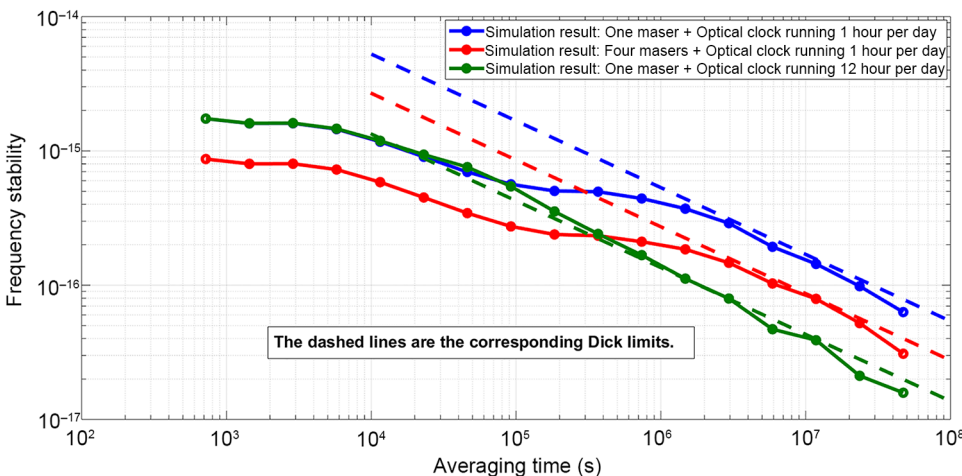


FIG. 5. Comparison between the Dick limits (dashed lines) and simulation results in [24].

in a steered time scale. We observe excellent agreement between these two analyses.

Reference [24] points out that there is an improvement of \sqrt{N} for an optical-clock-based time scale by using an ensemble of N masers rather than using a single maser. The Dick limit for the case of one maser and a four-maser ensemble are shown by the blue dashed line and the red dashed line in Fig. 5, respectively. Comparing these two dashed lines, we find the improvement is 2, consistent with the square root of the number of masers. Both the simulation results and the Dick limits demonstrate the advantage of the MTSOC architecture over the HMOC architecture.

Appendix B: Kalman-filter steering algorithm for optical-clock-based time scale

A Kalman filter is used to estimate the frequency and frequency drift of the free-running time scale AT1 with respect to the Yb clock, and AT1 is steered based on this estimate [24,47]. Here, we summarize the algorithm employed.

Equation (B1) is the system model, which predicts the state of the system at epoch $k+1$ based on its state at epoch k . Here, $X(k)$ is the estimate state vector of the system at epoch k , and $X(k+1|k)$ is the predicted state vector of the system at epoch $k+1$. For our system, X has two elements – the fractional frequency difference and the fractional frequency drift difference between AT1 and the Yb clock. Φ is the transition matrix, which links $X(k)$ and $X(k+1|k)$. u is the process noise, which is determined by the AT1 noise characteristics. Equation (B2) is the measurement model. The H matrix gives the relation between the state vector X and the measurement vector Z . For our system, the measurement vector Z is the average measured frequency difference between AT1 and the Yb clock during each operation period of the Yb clock and H is $(1 \ 0)$. v is the measurement noise.

$$X(k+1|k) = \Phi \cdot X(k) + u, \quad (\text{B1})$$

TABLE I. Error bars for the frequency stabilities in Fig. 4. The unit for numbers in this table is 10^{-16} . The 68.3% confidence level is used in this table to be consistent with the convention.

	AT1–UTC	AT1'–UTC	UTC(NIST) –UTC	UTC(PTB) –UTC	UTC(USNO) –UTC
5 days	(4.82, 6.16)	(4.62, 5.91)	(8.90, 11.96)	(4.14, 5.57)	(4.97, 6.56)
10 days	(3.32, 4.96)	(3.16, 4.51)	(9.41, 13.44)	(3.59, 5.36)	(3.99, 5.96)
15 days	(2.40, 3.98)	(2.32, 3.64)	(8.89, 13.94)	(2.70, 4.24)	(3.50, 5.79)
20 days	(1.94, 3.53)	(1.87, 3.19)	(7.08, 12.10)	(2.11, 3.61)	(3.49, 6.32)
25 days	(1.78, 3.64)	(1.34, 2.43)	(4.76, 8.65)	(1.95, 4.00)	(3.42, 6.35)
30 days	(1.95, 4.38)	(1.15, 2.26)	(3.46, 6.81)	(1.93, 4.35)	(2.97, 6.01)
35 days	(2.20, 5.36)	(1.05, 2.25)	(2.48, 5.30)	(2.00, 4.88)	(2.43, 5.35)
40 days	(2.46, 6.53)	(1.00, 2.33)	(1.86, 4.34)	(2.16, 5.75)	(1.94, 4.69)
45 days	(2.64, 7.62)	(0.88, 2.24)	(1.63, 4.16)	(2.37, 6.84)	(1.53, 4.07)
50 days	(2.67, 8.49)	(0.66, 1.85)	(1.29, 3.67)	(2.48, 7.86)	(1.51, 4.45)

$$Z(k+1) = H \cdot X(k+1|k) + v. \quad (\text{B2})$$

According to the principle of Kalman filter, the estimated state vector at epoch $k+1$ $X(k+1)$ can be calculated using Eq. (B3).

$$X(k+1) = X(k+1|k) + K \cdot [Z(k+1) - H \cdot X(k+1|k)], \quad (\text{B3})$$

where K is the Kalman gain matrix. From Eq. (B3), the estimated state vector is essentially a weighted average of the predicted state vector and the current measurement. The weight is determined by the Kalman gain matrix K . How to calculate K is out of the scope of this paper and can be found in the classical book [48]. To accommodate gaps in optical-clock data of at least 15 days, we implement an adjustment operation. We choose 15 days as a threshold from the empirical observation that AT1 exhibits clear random-walk noise behavior after 15 days and the knowledge that the Kalman filter cannot handle a random-walk process as well as a white-noise process. In the adjustment operation, we want to assign the weight of the prediction and the weight of the measurement based on their respective uncertainties. To be specific, the weight of the prediction should be proportional to $1/[\sigma_{\text{AT1}}^2(\tau = \text{gap time})]$, while the weight of the measurement should be proportional to $1/\sigma_{\text{Yb-AT1}}^2$ (see Sec. III for details about $\sigma_{\text{Yb-AT1}}$). Based on these weight calculations, we adjust the (1, 1) element of K accordingly. We emphasize that the gap-adjustment operation is a one-time operation. As long as an optical-clock data gap is shorter than 15 days, K is still calculated based on [48].

An intuitive understanding of this filter is as follows: the longer the Yb clock runs, the larger weight the run gets. Also, the longer the time interval between the previous run and the current run, the larger weight the current run gets. Once we know the estimated state vector $X(k+1)$, we steer AT1 by adjusting its frequency and frequency drift to generate AT1'.

Appendix C: Error bars for the frequency stabilities in Fig. 4

The data points in Fig. 4 are computed using STABLE 32 (Version 1.55), a popular scientific software for frequency stability analysis. In Fig. 4, we choose the “all-tau” option in STABLE 32, which provides the stability at every possible averaging-time value. Unfortunately, under the “all-tau” setting, STABLE 32 does not provide the error bars. Here, we calculate the error bars for each data point in Fig. 4, based on [49]. To be specific, according to Section 5.4.3 of [49], we can calculate the equivalent degrees of freedom for each data point. Then we use Eq. (45) of [49] to get the corresponding confidence intervals (i.e., error bars). The 68.3% confidence level is used to be consistent with the convention in the time and frequency community. Table I summarizes the results of the error-bar calculations.

- [1] I. A. Getting, Perspective/navigation – the Global Positioning System, *IEEE Spectrum* **30**, 36 (1993).
- [2] S. Bregni, *Synchronization of Digital Telecommunications Networks* (John Wiley & Sons, 2002).
- [3] X. Fang, S. Misra, G. Xue, and D. Yang, Smart grid – the new and improved power grid: a survey, *IEEE Commun. Surv. Tutor.* **14**, 944 (2011).
- [4] M. A. Lombardi, A. N. Novick, G. Neville-Neil, and B. Cooke, Accurate, traceable, verifiable time synchronization for world financial markets, *J. Res. Natl. Inst. Stand. Technol.* **121**, 436 (2016).
- [5] F. Riehle, Optical clock networks, *Nat. Photonics* **11**, 25 (2017).
- [6] A. Derevianko and M. Pospelov, Hunting for topological dark matter with atomic clocks, *Nat. Phys.* **10**, 933 (2014).
- [7] P. Adamson, *et al.*, Precision measurement of the speed of propagation of neutrinos using the MINOS detectors, *Phys. Rev. D* **92**, 052005 (2015).
- [8] B. Guinot and E. F. Arias, Atomic time-keeping from 1955 to the present, *Metrologia* **42**, S20 (2005).
- [9] The fractional frequency y is a dimensionless quantity defined as $[(\text{measured frequency}/\text{nominal frequency}) - 1]$. The frequency stability of a clock can be characterized by Allan deviation $\sigma = \sqrt{(1/2)\overline{(y_{i+1} - y_i)^2}}$ or the modified versions of Allan deviation; in general, the Allan deviation is a function of averaging interval. By definition, the fractional frequency difference between clock A and clock B y_{A-B} becomes $(\text{measured frequency of A}/\text{nominal frequency of A}) - (\text{measured frequency of B}/\text{nominal frequency of B})$.
- [10] L. Cutler, Fifty years of commercial caesium clocks, *Metrologia* **42**, S90 (2005).
- [11] R. Vessot, The atomic hydrogen maser oscillator, *Metrologia* **42**, 468 (2005).
- [12] W. Riley, *A History of the Rubidium Frequency Standard* (IEEE UFFC-S History, 2019).
- [13] J. Levine, Invited review article: The statistical modeling of atomic clocks and the design of time scales, *Rev. Sci. Instrum.* **83**, 021101 (2012).

- [14] A. Ludlow, An optical clock to go, *Nat. Phys.* **14**, 431 (2018).
- [15] N. Huntemann, C. Sanner, B. Lipphardt, C. Tamm, and E. Peik, Single-ion Atomic Clock with 3×10^{-18} Systematic Uncertainty, *Phys. Rev. Lett.* **116**, 063001 (2016).
- [16] C. W. Chou, D. B. Hume, J. C. J. Koelemeij, D. J. Wineland, and T. Rosenband, Frequency Comparison of Two High-Accuracy Al+ Optical Clocks, *Phys. Rev. Lett.* **104**, 070802 (2010).
- [17] M. Schioppo, R. Brown, W. McGrew, N. Hinkley, R. Fasano, K. Beloy, T. Yoon, G. Milani, D. Nicolodi, J. Sherman, N. Phillips, C. Oates, and A. Ludlow, Ultrastable optical clock with two cold-atom ensembles, *Nat. Photonics* **11**, 48 (2017).
- [18] N. Hinkley, J. A. Sherman, N. B. Phillips, M. Schioppo, N. D. Lemke, K. Beloy, M. Pizzocaro, C. W. Oates, and A. D. Ludlow, An atomic clock with 10^{-18} instability, *Science* **341**, 1215 (2013).
- [19] B. J. Bloom, T. L. Nicholson, J. R. Williams, S. L. Campbell, M. Bishof, X. Zhang, W. Zhang, S. L. Bromley, and J. Ye, An optical lattice clock with accuracy and stability at the 10^{-18} level, *Nature* **506**, 71 (2014).
- [20] C. Grebing, A. Al-Masoudi, S. Dörscher, S. Häfner, V. Gerginov, S. Weyers, B. Lipphardt, F. Riehle, U. Sterr, and C. Lisdat, Realization of a timescale with an accurate optical lattice clock, *Optica* **3**, 563 (2016).
- [21] H. Hachisu, F. Nakagawa, Y. Hanado, and T. Ido, Month-long real-time generation of a time scale based on an optical clock, *Sci. Rep.* **8**, 4243 (2018).
- [22] J. Lodewyck, S. Bilicki, E. Bookjans, J. Robyr, C. Shi, G. Vallet, R. L. Targat, D. Nicolodi, Y. L. Coq, J. Guéna, M. Abgrall, P. Rosenbusch, and S. Bize, Optical to microwave clock frequency ratios with a nearly continuous strontium optical lattice clock, *Metrologia* **53**, 1123 (2016).
- [23] F. Riehle, P. Gill, F. Arias, and L. Robertsson, The CIPM list of recommended frequency standard values: guidelines and procedures, *Metrologia* **55**, 188 (2018).
- [24] J. Yao, T. Parker, N. Ashby, and J. Levine, Incorporating an optical clock into a time scale, *IEEE Trans. Ultrason. Ferroelectr. Freq. Control.* **65**, 127 (2018).
- [25] C. Hagemann, C. Grebing, C. Lisdat, S. Falke, T. Legero, U. Sterr, F. Riehle, M. J. Martin, and J. Ye, Ultrastable laser with average fractional frequency drift rate below $5 \times 10^{-19}/\text{s}$, *Opt. Lett.* **39**, 5102 (2014).
- [26] T. Kessler, C. Hagemann, C. Grebing, T. Legero, U. Sterr, F. Riehle, M. J. Martin, L. Chen, and J. Ye, A sub-40-mHz-linewidth laser based on a silicon single-crystal optical cavity, *Nat. Photonics* **6**, 687 (2012).
- [27] W. McGrew, X. Zhang, H. Leopardi, R. Fasano, D. Nicolodi, K. Beloy, J. Yao, J. Sherman, S. Schaffer, J. Savory, S. Romisch, C. Oates, T. Parker, T. Fortier, and A. Ludlow, Towards adoption of an optical second: Verifying optical clocks at the SI limit, *Optica* **6**, 448 (2019).
- [28] T. M. Fortier, A. Bartels, and S. A. Diddams, Octave-spanning Ti: sapphire laser with a repetition rate $>1\text{GHz}$ for optical frequency measurements and comparisons, *Opt. Lett.* **31**, 1011 (2006).
- [29] J. Sherman and R. Jordens, Oscillator metrology with software defined radio, *Rev. Sci. Instrum.* **87**, 054711 (2016).

- [30] J. Yao, I. Skakun, Z. Jiang, and J. Levine, A detailed comparison of two continuous GPS carrier-phase time transfer techniques, *Metrologia* **52**, 666 (2015).
- [31] J. Yao, and J. Levine, in Proceedings of the 27th Institute of Navigation GNSS+ Conference (2014), pp. 1253–1260.
- [32] A. Bauch, S. Weyers, D. Piester, E. Staliuniene, and W. Yang, Generation of UTC(PTB) as a fountain-clock based time scale, *Metrologia* **49**, 180 (2012).
- [33] S. Peil, J. Hanssen, T. Swanson, J. Taylor, and C. Ekstrom, Evaluation of long term performance of continuously running atomic fountains, *Metrologia* **51**, 263 (2014).
- [34] J. Yao, T. E. Parker, and J. Levine, JY1 time scale: a new Kalman-filter time scale designed at NIST, *Meas. Sci. Technol.* **28**, 115004 (2017).
- [35] E. Arias, G. Panfilo, and G. Petit, Timescales at the BIPM, *Metrologia* **48**, S145 (2011).
- [36] K. Predehl, G. Grosche, S. Raupach, S. Droste, O. Terra, J. Alnis, T. Legero, T. Hansch, T. Udem, R. Holzwarth, and H. Schnatz, A 920-Kilometer optical fiber link for frequency metrology at the 19th decimal place, *Science* **336**, 441 (2012).
- [37] F. Giorgetta, W. Swann, L. Sinclair, E. Baumann, I. Coddington, and N. Newbury, Optical two-way time and frequency transfer over free space, *Nat. Photonics* **7**, 434 (2013).
- [38] M. Fujieda, T. Gotoh, F. Nakagawa, R. Tabuchi, M. Aida, and J. Amagai, Carrier-phase-based two-way satellite time and frequency transfer, *IEEE Trans. Ultrason. Ferroelectr. Freq. Control* **59**, 2625 (2012).
- [39] G. Petit, A. Kanj, S. Loyer, J. Delporte, F. Mercier, and F. Perosanz, 1×10^{-16} frequency transfer by GPS PPP with integer ambiguity resolution, *Metrologia* **52**, 301 (2015).
- [40] Z. Jiang, V. Zhang, Y. Huang, J. Achkar, D. Piester, S. Lin, W. Wu, A. Naumov, S. Yang, J. Nawrocki, I. Sesia, C. Schlunegger, Z. Yang, M. Fujieda, A. Czubla, H. Esteban, C. Rieck, and P. Whibberley, Use of software-defined radio receivers in two-way satellite time and frequency transfers for UTC computation, *Metrologia* **55**, 685 (2018).
- [41] E. Arias, D. Matsakis, T. Quinn, and P. Tavella, The 50th anniversary of the atomic second, *IEEE Trans. Ultrason. Ferroelectr. Freq. Control* **65**, 898 (2018).
- [42] J. Flury, Relativistic geodesy, *J. Phys. Conf. Ser.* **723**, 012051 (2016).
- [43] E. Kaplan, *Understanding GPS: Principles and Applications* (Artech House Publishers, Chapter 3, 1996).
- [44] T. Ely, E. Burt, J. Prestage, J. Seubert, and R. Tjoelker, Using the deep space atomic clock for navigation and science, *IEEE Trans. Ultrason. Ferroelectr. Freq. Control* **65**, 950 (2018).
- [45] L. Sliwczynski, P. Krehlik, J. Kolodziej, H. Imlau, H. Ender, H. Schnatz, D. Piester, and A. Bauch, Fiber-optic time transfer for UTC-traceable synchronization for telecom networks, *IEEE Commun. Stand. Mag.* **1**, 66 (2017).
- [46] A. Quessada, R. Kovacich, I. Courtillot, A. Clairon, G. Santarelli, and P. Lemonde, The Dick effect for an optical frequency standard, *J. Opt. B Quantum Semiclassical Opt.* **5**, S150 (2003).
- [47] J. Yao, J. Sherman, T. Fortier, H. Leopardi, T. Parker, J. Levine, J. Savory, S. Romisch, W. McGrew, X. Zhang, D. Nicolodi, R. Fasano, S. Schäffer, K. Beloy, and A. Ludlow, Progress on optical-clock-based time scale at NIST: simulations and preliminary real-data analysis, *NAVIGATION* **65**, 601 (2018).
- [48] A. Gelb, *Applied Optimal Estimation* (MIT Press, 1974).
- [49] W. Riley, *Handbook of Frequency Stability Analysis* (NIST Special Publication, 2008), Vol. 1065.